Journal of Ceramic Processing Research. Vol. 17, No. 9, pp. 974~977 (2016)

J O U R N A L O F
Ceramic Processing Research

Reduced structural anisotropy of (11$\bar{2}$2) semipolar GaN by using epitaxial lateral overgrowth

Han-Su Cho[a], Jonghee Hwang[b], Dae-Woo Jeon[b,*] and Jin-Woo Ju[a,*]

[a]*Photonics Device Research Center, Korea Photonics Technology Institute, Gwangju 500-779, Korea*

[b]*Korea Institute of Ceramic Engineering & Technology, 101 Soho-ro, Jinju 660-031, Gyeongsangnam-do, Korea*

NonpolarGaN and semipolarGaN have been studied for minimization of quantum confined Stark effect in c-plane GaN. A (1122) semipolarGaN layer was grown on m-plane sapphire substrates via epitaxial lateral overgrowth (ELOG) by metal organic chemical vapor deposition. Cross section filed emission scanning electron microscopy revealed a semipolarGaN layer with a smooth surface and an inverted trapezoid growth shape. For the layers not fully merged laterally, the structural anisotropic characteristics were reduced slightly. After merging laterally, the structural anisotropy was reduced significantly. In the [1100] directions of the X-ray beams, the full width at half maximum (FWHM)of the x-ray rocking curve of the (11$\bar{2}$2) plane was 1195 arcsec for semipolarGaN on unpatterned template and the FWHM decreased to 468 arcsec for merged semipolarGaN by ELOG.In addition, the optical properties of (1122) semipolarGaN using ELOG were improved significantly.

Key words: Epitaxial lateral overgrowth, MOCVD, SemipolarGaN, Refractive Index.

Introduction

Hexagonal GaN films grown along the [0001] c-axis exhibit spontaneous and strain-induced polarization, which decreases the device efficiency and luminescent output due to the quantum confined stark effect (QCSE) [1, 2]. To minimize the QCSE, non- and semipolarGaN have attracted considerable research attention [3-6]. In previous studies, the epitaxial layer presents a c-axis tilted by 58.4 ^{o} with respect to the surface normal and the internal polarization is reduced to 1/3 of the one existing in the c-plane GaN [7]. Several groups reported the formation of high quality nonpolar and semipolarGaN using the epitaxial lateral overgrowth (ELOG) method [8-10]. For ELOG methods, the SiO_2 stripes for the mask region were oriented parallel to the [1$\bar{1}$00] GaN m-axis because it has been demonstrated to be the only efficient orientation for defect reduction [11]. G. Nataf et al. reported improved semipolar (11$\bar{2}$2) GaN quality using asymmetric lateral epitaxy by metal organic chemical vapor deposition (MOCVD) [12]. Significant improvement in the crystalline quality was achieved by ELOG due to a decrease in the basal plane stacking fault using appropriate growth conditions, such as a low V/III ratio and low pressure. However, the azimuthal dependence of the full width at half maximum (FWHM) of the asymmetric ELOGGaN is not completely understood. The study of the anisotropy properties of semipolarGaN growth by MOCVD on a nominal m-plane sapphire has not been reported. This study examined the anisotropy of the semipolarGaN properties grown on m-plane sapphire using MOCVD.

*Corresponding author:
Tel : +82-55-792-2484, +82-62-605-9325
Fax: +82-55-792-2492, +82-62-605-9339
E-mail: dwjeon@kicet.re.kr, j2u2@kopti.re.kr

Experimental

The samples were grown on (10$\bar{1}$0) m-plane sapphire [less than 0.2 ^{o} miscut as measured by X-ray diffraction] substrates by MOCVD (Veeco D180 GaN reactor) with trimethylgallium and ammonia as the GaN and N precursors, respectively. Prior to growth, the sapphire substrates were heated to 1125 °C in hydrogen ambient for 5 min to remove any surface contamination. A 30 nm thick GaN nucleation layer was grown at 700 °C. The temperature was then increased to 1060 °C for 5 min to allow recrystallization, followed by the growth of a 2 μm thick-undoped (11$\bar{2}$2) semipolarGaN layer at 880 °C. The growth pressure was set between 200 and 300 Torr with a V/III ratio of 1400. After the first MOCVD growth, a 100 nm-thick SiO_2 film was deposited by plasma-enhanced chemical vapor deposition on the underlying (11$\bar{2}$2) semipolarGaN. A mask pattern consisting of SiO_2 stripes (7 μm wide) and the exposed semipolarGaN windows (4 μm wide) were processed using conventional photolithography and reactive ion etching.

The samples were then loaded into the MOCVD chamber to grow the ELOG semipolarGaN. A 3 μm (11$\bar{2}$2) semipolarGaN epi-layer was then re-grown on the un-patterned and stripe patterned templates by MOCVD (samples A and B, respectively). Sample C was prepared by growing a 6 μm thick (11$\bar{2}$2) semipolarGaN on the stripe patterned template. The

ELOG method by MOCVD led to fully coalesced and planar layers.

The crystal quality was examined by X-ray diffraction (XRD, Philips X'pert) using Cu Kα1 radiation (λ = 1.5406 Å). Cross section images of the $(11\bar{2}2)$ semipolarGaN were characterized using field emission scanning electron microscopy (FESEM). The root mean square (RMS) surface roughness of the films, as measured by atomic force microscopy (AFM), was measured over a 5 × 5 μm^2 surface area. The optical properties of the $(11\bar{2}2)$ semipolarGaN were measured at low and room temperature by photoluminescence spectroscopy (PL) using the 325 nm emission of a He-Cd laser with an excitation power up to 10 W/cm^2.

Results and Discussion

Fig. 1 shows FESEM images of the cross section and bird-eye view of the samples A, B and C. For sample A, the surface morphology was similar to the as-grown $(11\bar{2}2)$ semipolarGaN template surface. The surface shown in Fig.1(b) was quite rough. Figs. 1(d) and 1(f) shows SEM images of a bird's-eye view of the surface morphology of samples B and C, respectively. $(11\bar{2}2)$ semipolarGaN using the ELOG samples for samples B and C showed a flatter and smoother surface than sample A. The RMS surface roughness of samples A, B and C was 41.6, 8.9 and 17.7 nm, respectively. The AFM images are not shown. The growth rate of the +c-facet is normally slightly higher than other facets, so the asymmetric growth rate makes a rough surface, such as the surface of sample A [13]. However, for sample B, a smoother surface of $(11\bar{2}2)$ semipolarGaN using ELOG formed due to symmetric growth along +c-facet and +a-facet and the $(11\bar{2}2)$ flat surface was maintained by the $[1\bar{1}00]$ direction SiO_2 stripe pattern. With $(11\bar{2}2)$ semipolarGaN using ELOG for samples B and C, the initial growth mode with a symmetric growth rate and a $(11\bar{2}2)$ flat surface was confirmed as shown in the inset in Fig. 1(c). For sample C, the RMS surface roughness was slightly higher. A higher growth rate of the +c-facet occurred during asymmetric growth after merging. Fig. 1(c) shows the inverted trapezoid growth shape of sample B. As the crystal expands over the SiO_2 mask, preferentially along the +c direction and +a direction symmetrically, an inverted trapezoid growth shape formed to maintain the flat surface. In previous reports of $(11\bar{2}2)$ semipolarGaN grown by ELOG, it is very difficult to keep a flat surface [12] and merge between wings by only one step growth due to the asymmetric growth rate. However, the flat surface of sample B was formed only by one step growth. In Fig. 1(d), some voids are still present on the surface due to the imperfect film coalescence. Figs. 1(e) and 1(f) show SEM images of a cross section and bird-eye view of sample C. For sample C grown to a thickness of 6 μm, the edge of the inverted trapezoid shape of $(11\bar{2}2)$ semipolarGaN first reached the adjacent crystal edge. Further growth allows complete coalescence without voids.

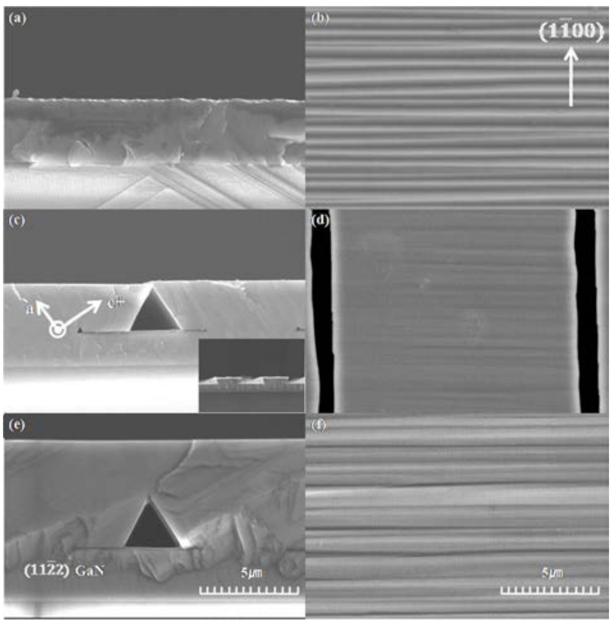

Fig. 1. Cross-sectional and plan view SEM images of $(11\bar{2}2)$ semipolarGaN for sample A (a,b), B (c,d) and C (e,f). The inset shows the cross-sectional SEM image of the initial growth mode with a symmetric growth rate and $(11\bar{2}2)$ flat surface.

Fig. 2 shows the FWHM of the x-ray rocking curve of the $(11\bar{2}2)$ plane as a function of the azimuth angle, which is defined as zero when the projection of the incident beam is parallel to the $[\bar{1}\bar{1}23]$ direction. The anisotropic feature marked as an M-shape dependence on the azimuth angle was observed for sample A. In the $[1\bar{1}00]$ and $[\bar{1}\bar{1}23]$ directions of the X-ray beams, the FWHM of sample A reached 1195 and 526 arcsec,

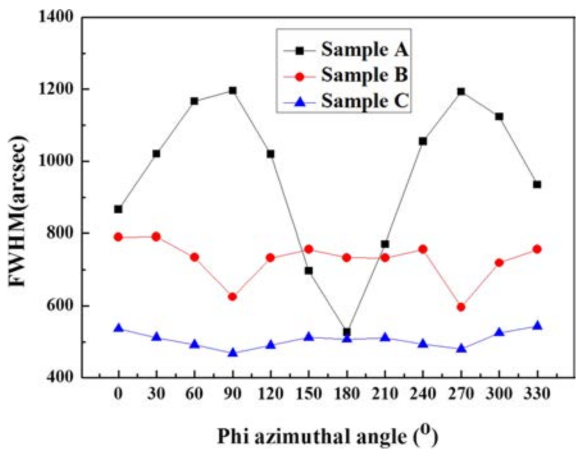

Fig. 2. FWHM of XRC of the $(11\bar{2}2)$ plane as a function of the azimuth angle, which is defined as zero when the projection of the incident beam is parallel to the (0001) direction. The inset shows the dependence of the XRC FWHM difference between two directions along the parallel to the $[1\bar{1}00]$ and $[\bar{1}\bar{1}23]$ directions of GaN.

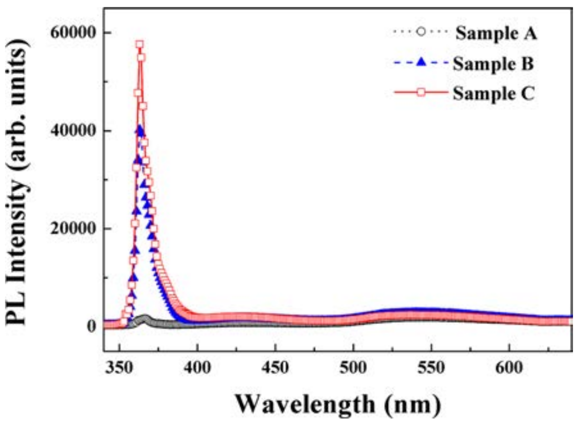

Fig. 3. Room temperature photoluminescence of (11$\bar{2}$2) semipolarGaN grown on unpatternedGaN template for sample A and (11$\bar{2}$2) semipolarGaN using the symmetric growth mode for samples B and C.

respectively. The structural anisotropy characterization could be attributed to the anisotropic in-plane growth rate, where the overall growth rate in the [0002] direction is higher than that in the [1$\bar{1}$00] direction [13]. Also, the anisotropic behavior is caused due to the anisotropic growth, most likely related to unavoidable defects with a specific distribution. This is to be expected that isotropic structure characteristic can be obtained in the semipolar growth with the improvement of crystalline quality [14]. For samples B and C, an inverse W-shape distribution was observed, and the omega FWHM value measured towards the [$\bar{1}\bar{1}$23] direction was higher than that towards the [1$\bar{1}$00] direction, as shown in Fig. 2. In the [1$\bar{1}$00] direction, the FWHM of sample B reached 624 arcsec. In a previous report, the (11$\bar{2}$2) semipolarGaN with fewer basal plane stacking faults was grown by asymmetric lateral epitaxy at low pressure using MOCVD [12]. However, the azimuthal dependence of the FWHM is not completely understood. The structural anisotropy property and transformation are believed to be related to asymmetric growth rate of nonpolar and semipolarGaN. For sample B, the FWHM value of the azimuth angle 0 ^{o} was similar to that at 180 ^{o}. This is in marked contrast to sample A. In addition, the structural anisotropy property was reduced slightly but still remained. The FWHM of the XRC of sample C revealed significantly reduced anisotropy. In the [1$\bar{1}$00] and [$\bar{1}\bar{1}$23] directions of the X-ray beams, the FWHM of the sample c reached 468 and 536 arcsec, respectively. The optimization growth conditions during (11$\bar{2}$2) semipolarGaN using ELOG were attributed to the reduced structural anisotropy.

Fig. 3 shows the room temperature PL spectra and relative intensities of samples A, B and C. All samples showed GaN near band-edge (NBE) recombination at approximately 360 nm. The near band edge PL relative intensity of samples B and C were 24 and 35 times higher, respectively, than that of sample A. At 363 nm of the GaN band edge, the PL intensity of sample C was stronger than that of sample B. In addition, the PL intensity of the yellow luminescence is significantly weak. For sample C, the structural anisotropy was not only reduced, but also the optical properties were improved considerably.

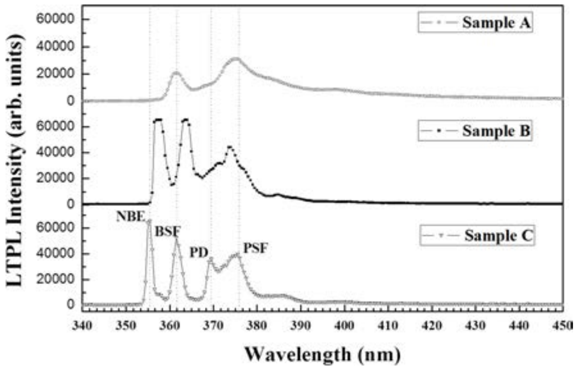

Fig. 4. Photoluminescence spectra of sample A, B and C at 10 K. Visible are the NBE as dominant peak and some defect related emission lines (e.g., BSF or PD).

Fig. 4 shows the low-temperature PL spectra measured on sample A, B, and C. The NBE emission of sample B and C is clearly separated from the basal plane stacking faults (BSF) emission peak with high PL peak intensity. The intensity ratio of NBE to BSF emission of sample C is higher than that of sample B, confirming that the crystal quality of sample C was improved by reducing the BSF after fully merged. The emission peak at ~361 nm observed on every sample is believed to be related to excitons bound to BSF [15], while the emission peak at 357.7 (sample B) and 355.5 nm (sample C) is related to NBE recombination [16]. The BSF emission of sample B occurs at 357.5 nm and is slightly lower (2 nm) than that of the sample A and C. This means the sample C maintains the same strain state as for the sample A, while the sample B tends to release the strain due to the large surface-to-volume ratio. After complete coalescence, the compressive strain was occurred again. Also, the several peaks (around 373 nm), usually assigned to (pyramidal) stacking faults (and partial dislocations) are still visible on every sample [17]. We assumed that these peaks did not make an impact on structural anisotropy of (11$\bar{2}$2) semipolarGaN.

Conclusions

This study examined the structural anisotropy of (11$\bar{2}$2) semipolarGaN using ELOG. The growth shape of (11$\bar{2}$2) semipolarGaN using ELOG formed an inverted trapezoid growth shape in the cross section image. The symmetric growth along the +c- and +a-facets by the [1$\bar{1}$00] direction SiO_2 stripe pattern was attributed to the flatter and smoother surface. For sample C, the edge of the inverted trapezoid shape of

$(11\bar{2}2)$ semipolarGaN reached the adjacent crystal edge and further growth allowed complete coalescence. XRD of sample C showed that the anisotropy had been reduced significantly. This improvement was also confirmed by PL measurements. The sample C shows high band edge emission intensity with a low FWHM, and a reduced BSFs related emission intensity. The structural and optical properties of $(11\bar{2}2)$ semipolarGaN were improved significantly by the ELOG growth.

Acknowledgments

This work was supported by Basic Science Research Program through the National Research Foundation of Korea (NRF) funded by the Ministry of Education (No. 2015R1D1A1A01060417).

References

1. J. Piperek, R. Farrell, S. DenBaars, and S. Nakamura, IEEE Photon. Technol. Lett. 18 (2006) 7.
2. T. Takeuchi, H. Amano, and I. Akasaki,Jpn. J. Appl. Phys. 39 (2000) 413.
3. H.Y. Song, J.S. Kim, E.K. Kim, Y.G. Seo, and S.M. Hwang, Nanotechnology 21 (2010) 134026.
4. P. De Mierry, N. Kriouche, M. Nemoz, S. Chenot, and G. Nataf, Appl. Phys. Lett. 96 (2010) 231918.
5. F. Tendille, P. De Mierry, P. Vennéguès, S. Chenot, and & M.Teisseire, J.Cryst. Growth404 (2014) 177.
6. Y. Ryu, J. Jeong, J. Jang, K. Lee, D. Min, J. Kim, M. Kim, S. Moon, G. Yoo, and O. Nam, J. Ceram. Process. Res. 14 (2013) 587.
7. A.E. Romanov, T.J. Baker, S. Nakamura, and J.S. Speck, J. Appl. Phys. 100 (2006) 023522.
8. J.J. Huang, K.C. Shen, W.Y. Shiao, Y.S. Chen, T.C. Liu, T.Y. Tang, C.F. Huang, and C.C. Yang, Appl. Phys. Lett. 92 (2008) 231902.
9. X. Ni, U. Ozgur, A.A. Baski, H. Morkoc, L. Zhou, D.J. Smith, and C.A. Tran, Appl. Phys. Lett. 90 (2007) 182109.
10. B. Humphreys, T. Zhang, C. Griffiths, and T. Wang, ChinaSSL (2013) 52.
11. Z. Bougrioua, M. Laugy, P. Vennergues, I. Cestier, T. Guhne, E. Frayssinet, P. Gibart, and M. Leroux, Phys. Stat. Sol. [A] 204 (2007) 282.
12. P. de Mierry, N. Kriouche, M. Nemoz, and G. Nataf, Appl. Phys. Lett. 92 (2009) 191903.
13. H.M. Wang, C.Q. Chen, Z. Gong, J.P. Zhang, M. Gaevski, M. Su, J.W. Yang, and M. A. Khan, Appl. Phys. Lett. 84 (2004) 499.
14. T.B. Wei, Q. Hu, R.F. Duan, X.C. Wei, Z.Q. Huo, J.X. Wang, Y.P. Zeng, G.H. Wang, and J.M. Li, J. Cryst. Growth 311 (2009) 4153.
15. R. Liu, A. Bell, F.A. Ponce, C.Q. Chen, J.W. Yang, and M.A. Khan, Appl. Phys. Lett. 86 (2005) 021908.
16. T. Guhne, Z. Bougrioua, P. Vennegues, and M. Leroux, J. Appl. Phys. 101 (2007) 113101.
17. R. Kroger, in Nitrides with Nonpolar Surfaces: Growth, Properties, and Devices, edited by T. Paskova (Wiley, New York, 2008) p.287.